Desalination and Water Treatment
www.deswater.com
doi: 10.1080/19443994.2015.1088896

57 (2016) 18062–18075
August

Taylor & Francis
Taylor & Francis Group

Comparison of Fe/surfactant improved montmorillonite: adsorbing and in situ decomposing methylene blue and recycling use

Xueping Liu[a], Xiaohui Jiang[a,*], Zhengjun Cheng[a], Limei Zhou[a], Yunwen Liao[a], Ming Duan[b], Qiang Pu[c]

[a]*Chemical Synthesis and Pollution Control Key Laboratory of Sichuan Province, China West Normal University, Nanchong, Sichuan 637009, P.R. China, Tel. +86 18090574469; email: 935846919@qq.com (X. Liu), Tel. +86 817 2314508; Fax: +86 817 2568625; email: jxh2314508@163.com (X. Jiang), Tel. +86 13084335453; email: ncczj@yahoo.com.cn (Z. Cheng), Tel. +86 15881769565; email: Lmz860@126.com (L. Zhou), Tel. +86 18990701813; email: liao-yw@163.com (Y. Liao)*
[b]*State Key Laboratory of Oil and Gas Reservoir Geology and Exploitation, Southwest Petroleum University, Chengdu, Sichuan 610500, P.R. China, Tel. +86 13981892218; email: mduan@swpi.edu.cn*
[c]*China Petroleum Engineering Co., Ltd Southwest Company, Chengdu, Sichuan 610213, P.R. China, Tel. +86 13402854621; email: puq@qq.com*

Received 19 October 2014; Accepted 21 August 2015

ABSTRACT

Montmorillonite (MMt) was intercalated by polymeric Fe, or by N-ethyl dodecyl nicotinate bromide (EDNB), or by both. The improved MMt designated as Fe/MMt, EDNB/MMt, and EDNB/MMt/Fe, respectively. A comparison was performed on the improved MMt in the uptake and in the degradation of methylene blue (MB) as well as in the recycling use. The results showed that EDNB/MMt adsorbed more MB than the other two; however, Fe/MMt and EDNB/MMt/Fe acted faster than the former. The adsorption of MB on the three adsorbents followed Langmuir isotherm and pseudo-second-order kinetics. In addition, MB adsorbing on EDNB/MMt was also well described by intraparticle diffusion model. MB removal by EDNB/MMt experienced an endothermic and entropy driving process, but an exothermic and entropy declining process by the other two. pH of the solution affected MB removal. When pH of the solution is high than 10, MB uptake diminished on Fe/MMt and EDNB/MMt/Fe; however, it slightly increased on EDNB/MMt. MB could be decomposed by Fenton reagent on the improved MMt, and the adsorbents could be reused. By coupling the adsorption and degradation *in situ* by H_2O_2/Fe^{2+} or Fe^{3+}, MB removal by Fe/MMt and EDNB/MMt/Fe was almost maintained in the ten cycles. So, present work deepens the understanding of modified MMt in the application of dye wastewater treatment.

Keywords: Improved MMt; *In situ* decomposition; MB adsorption; Recycling

1. Introduction

Methylene blue (MB) is widely used for dyeing paper, hair, cotton, and wool. It is often lost as waste effluent in the dyeing process and causes environment pollution. So, it must be removed prior to being discharged [1]. The chemical structure of MB is complicated and very stable to light and oxidation and biodegradation [2,3]. Photochemical degradation [4],

*Corresponding author.

chemical oxidation [5], biodegradation [6], and adsorption [7–10] have been applied to removing MB from wastewater, of which adsorption is the effective, economical, and easy way.

Montmorillonite and modified MMt are widely used as adsorbents in dye wastewater treatment due to the replaceable interlayer cations for modification and the high efficiency for contaminant removal [11]. Almeida and his colleagues investigated MB uptake by pristine MMt. The result unveiled that 71.9% of MB was removed at 45˚C [12]. In order to enhance MB uptake of the clay, MMt has been modified with cationic surfactants [13] and polymeric metal ions [14]. These modifications improve the hydrophobicity, the specific surface area, and the pore volume of the clay. So, the contaminant uptake of the clay is enhanced. Gil and his colleague reported that MB uptake capacity of zirconium-pillared MMt was higher than that of aluminum-pillared MMt, and both were higher than that of MMt [15]. The combination of metal ions pillar and surfactant intercalation endows the modified MMt with better hydrolytic stability and with higher uptake ability for organic pollutants [16,17].

Although lots of modified MMts are engaged in the research of waste treatment, a comparison of these modified MMt in pollutant removal is seldom reported, which is important for the practical application of modified MMt. Therefore, in this study, a new surfactant-intercalated MMt (organic clay), Fe pillared one (inorganic clay) and Fe-pillared surfactant-MMt (inorganic organic clay) are prepared, and a comparison is carried out in MB uptake, *in situ* decomposition of MB, and in recycling utilization of the three adsorbents.

2. Materials and experiments

2.1. Materials

Analytical grade of nicotinic acid, thionyl chloride, dodecanol, bromoethane, ferrous ammonium sulfate, hydrogen peroxide, and MB were purchased from Chengdu Kelong Chemical Reagent Co., China, and used as supplied. The montmorillonite used has a cation exchange capacity of 60.00 mequiv/100 g. Distilled water was used in all experiments.

MB solutions of different concentrations (400–1,600 mg/L) were prepared by dissolving MB in distilled water. The concentrations of MB were determined by UV–vis spectrometry on Shimadzu UV3600 spectrophotometer at 664 nm. The calibration curve was done according to the spectra of standard solutions (1–8 mg/L) at pH 6.

2.2. Synthesis of EDNB

EDNB is prepared according to the procedure presented in Fig. 1.

Nicotinic acid (0.1 mol) and thionyl chloride (50 mL) were mixed, and refluxed for 4 h. Excess thionyl chloride was removed by distillation under vacuum, and needle-like nicotinoyl chloride was attained. Then, dodecanol was dripped into the flask containing nicotinoyl chloride, mixed and refluxed for 4 h. The pH of the solution was carefully adjusted to 7–8. The organic layer was separated, dried overnight on anhydrous $MgSO_4$. Finally, $MgSO_4$ was removed by filtration, and dodecyl nicotinate was obtained by vacuum distillation.

The ester was mixed with bromoethane (1:5) in acetonitrile (30 mL) and refluxed for 8 h under agitation. Then, the mixture was stood for hours to precipitate thoroughly. The coarse product was recrystallized in petroleum ether and CH_3OH (5:1) at least three times. The target compound, N-ethyl dodecyl nicotinate bromide, was collected with a yield of 61%. The structure was confirmed by ^1H NMR, ^{13}C NMR, and FTIR (Figs. S1–S3).

2.3. Preparation of the adsorbents

A total of 2.0 g of MMt was dispersed in water for 12 h at 60˚C. 80 mL of EDNB (2 mol/L) was added to the dispersion. The mixture was kept stirring for 2 h and aged for 24 h at 60˚C. The precipitate was separated by suction and washed several times with distilled water until free of bromides, as indicated by $AgNO_3$ test. Then, EDNB/MMt was obtained.

The Fe-pillaring solution was prepared as follows: Na_2CO_3 solution was added dropwise into the $FeCl_3{\cdot}6H_2O$ solution under vigorous stirring at 60˚C for 2 h, and the mixture was aged for 24 h.

The Fe-pillaring solution was added dropwise into MMt dispersion or into EDNB/MMt suspension, respectively. The mixture was stirred for 2 h and aged for 24 h at 60˚C. Then, Fe/MMt and EDNB/MMt/Fe were collected by filtration, respectively.

These modified MMts were dried overnight at 80˚C and activated at 110˚C for 2 h before use.

2.4. The batch test

The pH of 20 mL of MB solution (800 mg/L of MB for EDNB/MMt and 600 mg/L for Fe/MMt and EDNB/MMt/Fe) was carefully adjusted by adding a small amount of HCl or NaOH solution. The solution was mixed with 40 mg of the modified MMt, agitated for 1 h at certain temperature (25–65˚C), and then, the

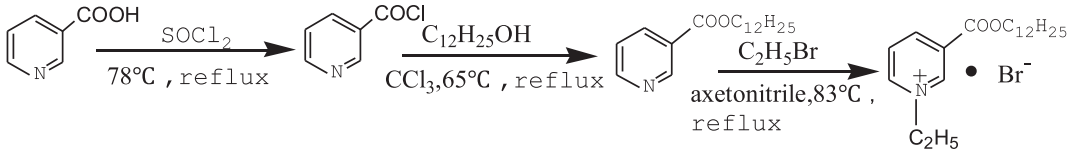

Fig. 1. The synthetic route of EDNB.

mixture was centrifuged. The absorbance of supernatant was measured by UV–vis spectrometer. The concentration of MB in the supernatant was obtained according to the standard curve in Fig. S4.

The removal efficiency (R %) and the amounts of MB adsorbed at equilibrium (q_e, mg/g) are calculated according to the following expressions:

$$R\ \% = \frac{(C_0 - C_e)}{C_0} \times 100 \quad (1)$$

$$q_e = \frac{(C_0 - C_e)V}{m} \quad (2)$$

where C_0 and C_e (mg/L) are the concentrations of MB solution before and at the adsorption equilibration, respectively. m is the mass of adsorbent, and V is the volume of MB. C_e is obtained by the standard curve and equation.

2.5. Adsorption kinetics test

The adsorption kinetics of MB were conducted by equilibrating 400 mg of the improved MMt in 200 mL of MB solution (600 mg/L for Fe/MMt and for EDNB/MMt/Fe; 800 mg/L for EDNB/MMt) at different time intervals and at 298–338 K.

2.6. Adsorption isotherms measurement

40 mg of the modified MMT was put into 20 mL of MB solutions (400–1,600 mg/L), mixed thoroughly under stirring and maintained for 1 h at 298–338 K.

2.7. In situ decomposition of MB and recycling of adsorbents

The precipitate was separated from the solution by centrifugation when the adsorption was ended, mixed with 20 mL of 30% H_2O_2 and 10 mg of $(NH_4)_2SO_4 \cdot FeSO_4 \cdot 6H_2O$, and stirred at 60℃ for 3 h until the blue color faded. Then, the precipitate was isolated by centrifugation, washed with distilled water and centrifuged again for times, dried overnight at 80℃, and activated at 110℃ for 2 h. And then, the adsorption for MB was done as that described in Section 2.4. MB adsorption and *in situ* oxidation on the modified MMt were performed ten times.

3. Results and discussion

3.1. Characterization of the improved MMt

The structure of the adsorbents was characterized. X-ray diffraction patterns (XRD) shows a basal spacing of 1.145 nm for crude MMt and of 1.335 nm for EDNB/MMt, indicating the intercalation of the surfactant in MMt (Fig. 2). However, the d_{001} peak of Fe/MMt and EDNB/MMt/Fe disappears. Pillared clay that exhibits no (0 0 1) diffraction has been referred to as "delaminated clay." The reduction in diffractogram of Fe/MMt and EDNB/MMt/Fe is probably due to delamination of MMt layers by hydroxyl iron ions [18]. The thermogravimetric analysis of the modified MMt is illustrated in Fig. 3. The peak at 104℃ belongs to the loss of water molecules adsorbed on Fe/MMt, suggesting the hydrophilicity of this pillared clay. However, this peak disappears in the curves for EDNB/MMt and EDNB/MMt/Fe, indicating that the intercalation of the surfactant endows

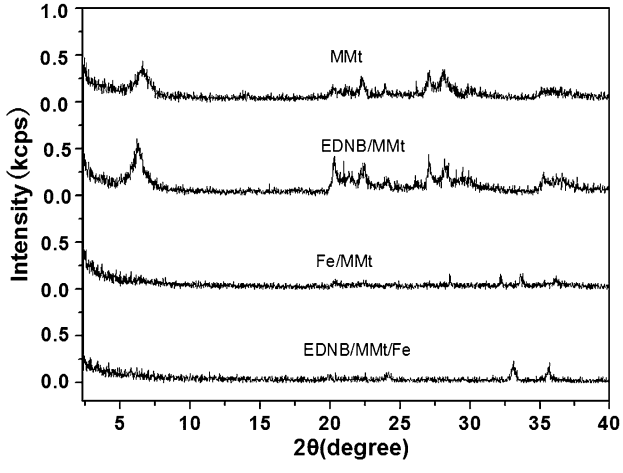

Fig. 2. Powder XRD patterns of the improved MMt.

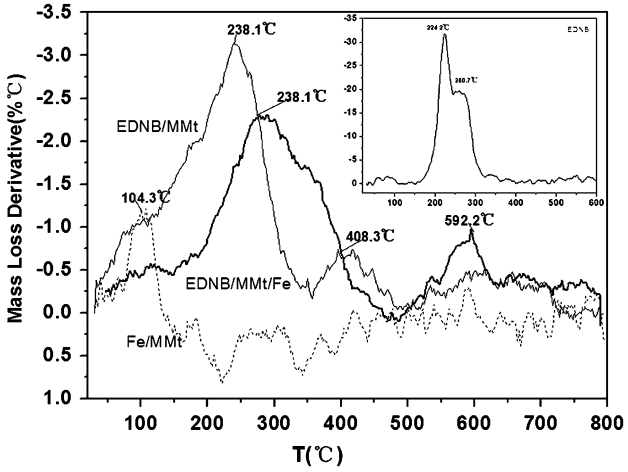

Fig. 3. Differential thermogravimetric curves of the improved MMt (inset for EDNB).

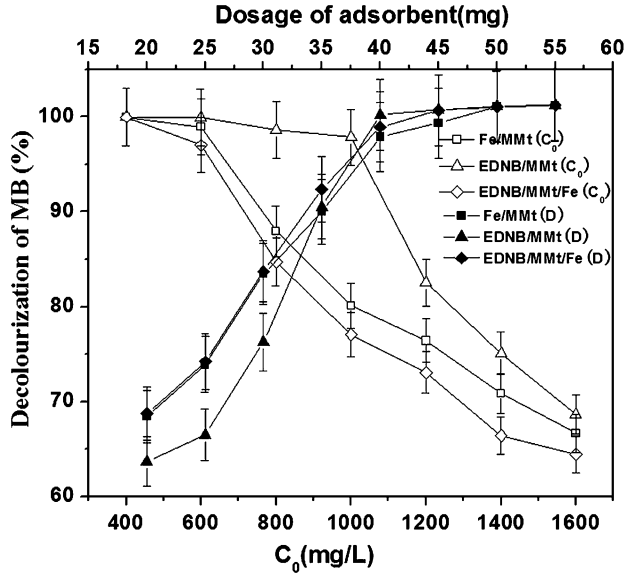

Fig. 4. The dependence of decolorization % on the dosage of the adsorbents and on the initial concentration of MB, respectively (condition: 800 mg/L of MB for EDNB/MMt and 600 mg/L for Fe/MMt and EDNB/MMt/Fe, 40 mg of the adsorbents, 25℃ and 1 h).

MMt and Fe/MMt with hydrophobicity. Comparing the curves of EDNB/MMt and EDNB/MMt/Fe with that of EDNB (the inset) specifies that the mass loss temperature of EDNB/MMt (at 238 and 408℃) is higher than that of EDNB (224 and 250℃) and that the mass loss temperature of EDNB/MMt/Fe is much higher (280 and 592℃), which indicates the strong interaction between EDNB and MMt, and the stronger interaction of EDNB with Fe-pillared MMt. FTIR spectra of the adsorbents evidence the specific absorption bands of EDNB (the vibration of CH_3 and CH_2 at 2,924.82 and 1,453.98 cm^{-1} and that of the ester group at 1,740 cm^{-1}) in EDNB/MMt and EDNB/MMt/Fe, hinting the existence of the surfactant in the MMt (Fig. S5).

3.2. The optimization of MB adsorption on the modified MMt

The effect of the adsorbent dosage on MB uptake is graphed in Fig. 4. It is shown that the MB uptake rises rapidly with increasing the adsorbent dosage from 20 to 40 mg. The increased MB uptake can be ascribed to the augmented available adsorption sites because more adsorbents supply more sites for MB adsorption [19]. With further increase of adsorbent dosage, MB uptake by the adsorbents levels out, hinting that the balance of adsorption and desorption is established. Furthermore, the figure also manifests that the adsorption capacity of EDNB/MMt toward MB is much bigger than those of EDNB/MMt/Fe and Fe/MMt. Taken into account the structure features of EDNB, MB and modified MMt, we speculate that besides electrostatic attraction, the hydrophobic interaction and π–π stacking play roles in the adsorption, which is responsible for higher MB uptake on EDNB/MMt.

It can be seen that the MB removal by EDNB/MMt/Fe and Fe/MMt declines a little in MB concentration range of 400–600 mg/L and then drops drastically with the incremental concentration of the dye (Fig. 4). However, it is almost unchanged by EDNB/MMt in the concentration of 400–1,000 mg/L of MB, and then, it declines gradually.

The contact time affects MB adsorption on the adsorbents. Fig. 5 unveils that decolorization% of MB increases with prolonging the reaction time. MB uptake reaches the maximum in ten minutes for EDNB/MMt/Fe and for Fe/MMt. However, it takes about 1 h for MB adsorption up to the maximum value on EDNB/MMt. So EDNB/MMt/Fe and Fe/MMt act faster with MB than EDNB/MMt in the adsorption process.

The decolorization of MB by the adsorbents is weakly affected by temperature (Fig. S6). MB removal declines slightly by EDNB/MMt/Fe and Fe/MMt. However, it rises a little by EDNB/MMt in 25–65℃.

MB removal efficiency by EDNB/MMt/Fe and Fe/MMt is kept at pH of 3–10 (Fig. S7), and it declines a little at pH 11. However, it increases abruptly at pH 4–6 by EDNB/MMt, but afterward, it almost levels out in the pH range of 6–11. Such trend of MB uptake

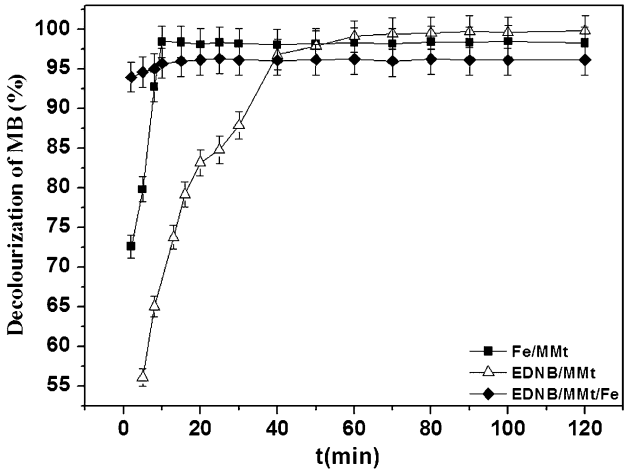

Fig. 5. The relationship between decolorization % of MB and contact time (condition: 400 mg of adsorptions, the concentrations of MB are 800 mg/L for EDNB/MMt, and 600 mg/L for Fe/MMt and EDNB/MMt/Fe, 25°C).

may be correlated with the variation of zeta potential of the adsorbent dispersion in the pH range.

The zeta potential for Fe/MMt is variable with pH value of the solution [20,21]. Fig. 6 illustrates that zeta potential of all the adsorbent dispersion varies more negatively with increasing pH. EDNB/MMt presents the lowest zeta potential values, Fe/MMt the medium, and EDNB/MMt/Fe the highest. As reported in literatures [22–24], the overall particle charge of MMt is always negative. However, negatively and positively charged parts on the surface of clay minerals coexist simultaneously under acidic conditions. The iron incorporation on the clay mineral structure changes the surface properties with incorporation of metallic

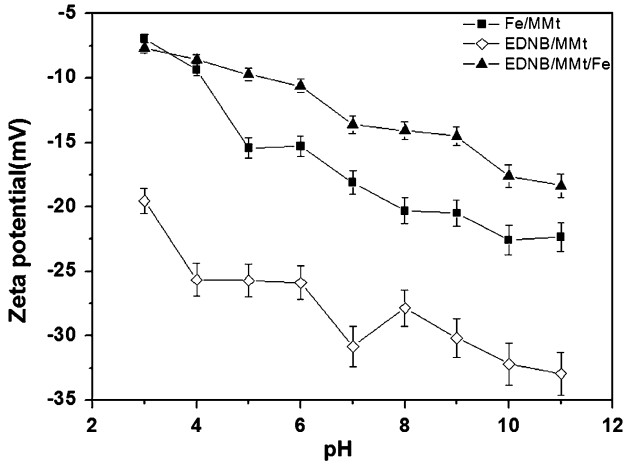

Fig. 6. The relationship between zeta potential and the pH of the adsorbent solution.

centers of iron(III), which resulting more positive values for Fe/MMt. This Fe^{3+} in Fe/MMt surface is coordinated to oxygen atoms, and the existed state may be protonated $(-FeOH)^+$, neutral (=FeOH) or deprotonated $(=FeO)^-$ depending on the pH of the solution [18]. Therefore, Fe/MMt shows the zeta potential-pH dependence fashion. The zeta potential of EDNB/MMt becomes more negative in alkaline solution. The reason lies in the hydrolysis of EDNB in alkaline solution which produces anions ($-COO^-$) and shifts zeta potential toward more negative direction. The zeta potential for EDNB/MMt/Fe is less negative than that of Fe/MMt. According to DTG curves in Fig. 3, the temperature for the weight loss of EDNB is much higher in EDNB/MMt/Fe than in EDNB/MMt, hinting the stronger interaction between the surfactant and the polymeric iron ion. We suppose, under alkaline condition, the $-COO^-$ in EDNB may combine with Fe^{3+}, the anions, $-COO^-$ and $(=FeO)^-$, are reduced, so, the zeta potential of EDNB/MMt/Fe is higher than that of Fe/MMt.

Therefore, the more and more negative zeta potential of the improved MMt dispersion with the elevated pH value is responsible for the incremental MB removal on EDNB/MMt and for the unchanged MB removal on the other two adsorbents.

3.3. Adsorption kinetics

The time profiles of MB uptake are depicted in Fig. S8 by the improved MMt. The kinetics analysis can predict the adsorption rate and adsorption mechanism. The pseudo-first-order (Eq. (3)), pseudo-second-order (Eq. (4)), and Elovich (Eq. (5)) equations are employed to analyze the experimental data [25].

$$\ln(q_e - q_t) = \ln q_e - k_1 t \tag{3}$$

$$\frac{t}{q_t} = \frac{1}{k_2 q_e^2} + \frac{t}{q_e} \tag{4}$$

$$q_t = \frac{\ln \alpha\beta}{\beta} + \frac{\ln t}{\beta} \tag{5}$$

where q_t and q_e (mg/g) are the amounts of MB adsorbed at time t and at equilibrium, respectively; k_1 and k_2 are the adsorption rate constants in the pseudo-first-order equation and pseudo-second-order equation, respectively; α is the initial adsorption rate, and β is related to surface coverage and activation energy of chemiadsorption.

The data fitting according to the pseudo-second-order model is plotted in Fig. 7 for MB adsorbed on

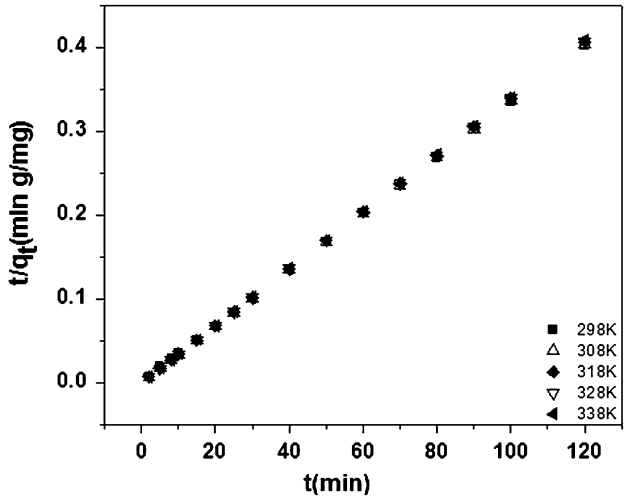

Fig. 7. The pseudo-second-order kinetics plots for MB absorption on EDNB/MMt.

EDNB/MMt (plots for the other two adsorbents and those by fittings according to other kinetics models in Figs. S9–S11). The kinetics parameters for MB adsorbing onto the improved MMt are tabulated in Table 1. The pseudo-second-order model is the most suitable one for describing the adsorption because R^2 values are close to 1 and the theoretical $q_{e,cal}$ is in good agreement with the $q_{e,exp}$. In addition, chi-square (χ^2), a criterion for the fitting quality, is quite small, indicating that experimental data fit better to the model.

The adsorption rate constant, k_2, is rising within the temperature range of 298–338 K for all the three adsorbents (Table 1). And it is worthy of attention that k_2 value is in the order of k_2 (Fe/MMt) > k_2 (EDNB/MMt/Fe) > k_2 (EDNB/MMt). The larger the k_2 value is, the faster MB adsorbs on the adsorbent. This supports well the experiment results.

As we known, the external mass transfer and intraparticle diffusion are crucial in rate determination of the adsorption process, so the data obtained by time course are fitted to Weber−Morris intraparticle diffusion model [26,27].

$$q_t = K_d t^{1/2} + I \tag{6}$$

where q_t is the amount of MB adsorbed at time t (min), and K_d is the rate constant for intraparticle diffusion. Values of I give an idea about the thickness of the boundary layer, i.e. the larger the I value is, the greater the boundary layer effect will be. K_d and I can be obtained from the slope and the intercept of the linear plots of q_t vs. $t^{1/2}$, respectively.

Fig. 8 plots the data fitting for MB sorbing on EDNB/MMt according to Eq. (5) (those on EDNB/MMt/Fe and Fe/MMt in Fig. S12). It is obviously that these plots do not pass through the origin, indicating that the intraparticle diffusion is involved in the adsorption process, but not the sole rate-limiting step [28]. Piecewise linear regression of data represents that plots of q_t vs. $t^{1/2}$ exhibit three distinct regions. External mass transfer appears at the first 0–8 min for MB transferring fast from liquid phase to the outer surface of EDNB/MMt/Fe and Fe/MMt, and binding with the active sites on the surface. Comparison of the plots specifies that the first stage lasts 16 min for MB onto EDNB/MMt, hinting a slower MB adsorption on EDNB/MMt. Then, intraparticle diffusion of MB toward the interior sites of EDNB/MMt/Fe and Fe/MMt is fulfilled quickly, too quickly at elevated temperature to distinguish the stage, so that only two stages can be clearly discerned, the same as in reference [15]. However, it happens gradually during a period of 16 min for MB diffusing in the inter surface of EDNB/MMt. The adsorption is finally equilibrated accompanied by slower intraparticle diffusion due to extremely low MB concentrations in solution [29].

Table 2 and Tables S1 and S2 summarize the corresponding parameters. I_1 values are positive and rise with the raising temperatures, suggesting that the resistance to the external mass transfer is enhanced as the thickness of the boundary layer increases [30]. K_d declines slowly with the elevated temperature for MB adsorbed on EDNB/MMt. However, for MB adsorbing on EDNB/MMt/Fe and Fe/MMt, K_{d1} and K_{d2} decreased rapidly while K_{d3} increase a little with temperature. Generally, K_{d1} for MB adsorption on the three adsorbents is larger than K_{d2}, signifying that intraparticle diffusion controls the MB adsorption on the modified MMt [31].

3.4. Adsorption isotherms

Langmuir model, Freundlich model, and Dubinin–Radushkevich model have been utilized to describe the adsorption equilibrium between the solution and the solid phases [32,33].

$$\text{Langmuir isotherm: } \frac{C_e}{q_e} = \frac{1}{bq_m} + \frac{C_e}{q_m} \tag{7}$$

$$\text{Freundlich isotherm: } ln\ q_e = \ln\ K_F + \frac{1}{n} \ln\ C_e \tag{8}$$

$$\text{Dubinin–Radushkevich isotherm: } \ln\ q_e = \ln\ q_m - K'\varepsilon^2 \tag{9}$$

Table 1
Kinetics parameters from pseudo-second-order kinetic model for MB adsorption on the improved MMt

	EDNB/MMt					Fe/MMt					EDNB/MMt/Fe				
T (K)	k_2 (g/(mg min))	$q_{e,cal}$ (mg/g)	R^2	$\chi^2 \times 10^4$	$q_{e,exp}$ (mg/g)	k_2 (g/(mg min))	$q_{e,cal}$ (mg/g)	R^2	$\chi^2 \times 10^4$	$q_{e,exp}$ (mg/g)	k_2 (g/(mg min))	$q_{e,cal}$ (mg/g)	R^2	$\chi^2 \times 10^4$	$q_{e,exp}$ (mg/g)
298	0.0006	413.2	0.999	0.1	399.3	0.0148	299.40	1	6.7	298.7	0.01048	295.8	1	37.5	295.1
308	0.0009	409.8	0.999	0.1	399.5	0.0762	297.62	1	4.1	297.2	0.02644	294.1	1	24.2	293.4
318	0.0011	408.1	1	0.1	399.8	0.0864	294.99	1	1.2	295.4	0.03318	294.1	1	15.1	294.3
328	0.0014	406.5	1	4.4	399.8	0.0946	294.99	1	0. 1	294.8	0.04024	292.4	1	7.4	291.7
338	0.0049	401.6	1	0.3	399.8	0.1171	294.12	1	1.3	293.9	0.04955	289.0	1	1.3	288.5

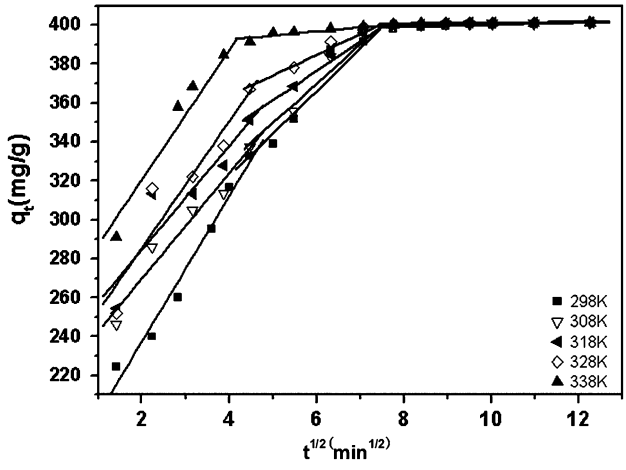

Fig. 8. Weber–Morris kinetic model plots for MB adsorption on EDNB/MMt.

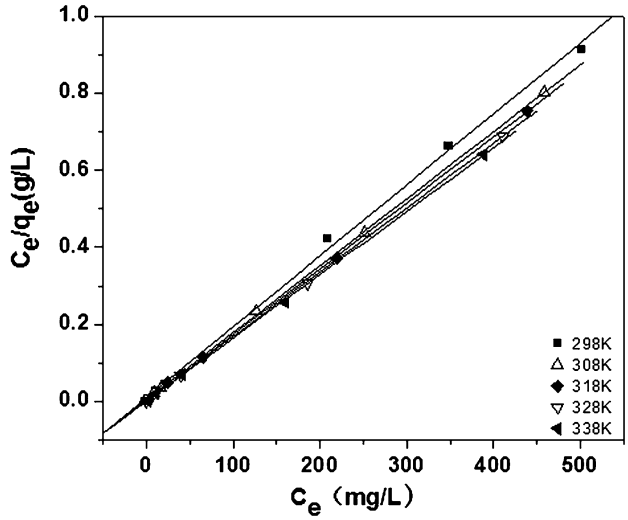

Fig. 9. Langmuir isotherm plots for MB adsorption on EDNB/MMt.

where q_m represents the monolayer adsorption capacity, and b is the Langmuir isotherm coefficient. k_F and n are Freundlich constants; ε is Polanyi potential ($\varepsilon = RT\ln(1 + 1/C_e)$), R is the gas constant, and T is the temperature (K). The dependence of K' on mean adsorption energy (E) is expressed as follows:

$$E = \frac{1}{\sqrt{2K'}} \tag{10}$$

Moreover, based on further analysis of Langmuir equation, the separation factor R_L (a dimensionless parameter) is defined by the following formula:

$$R_L = \frac{1}{1 + bC_0} \tag{11}$$

Data fitting demonstrates that Langmuir isotherm describes better the MB adsorption on ENDA/MMt with the highest R^2 and with good agreement of $q_{m,cal}$ and $q_{m,exp}$ (Fig. 9; the plots for the other two adsorbents and those according to other isotherms in Figs. S13–S15). The parameters from the data fitting are given in Table 3 and Tables S3 and S4. The value of R_L can predict if the adsorption process is unfavorable ($R_L > 1$), favorable ($R_L < 1$), linear ($R_L = 1$), or irreversible ($R_L = 0$) [34,35]. All R_L values are smaller than 1, implying that MB is favorably removed by the three modified MMt. R_L rises with elevating the temperature for MB adsorbing on EDNB/MMt, suggesting that higher temperature favors the adsorption. However, R_L declines with temperature for MB adsorption on EDNB/MMt/Fe and Fe/MMt, manifesting an unfavorable adsorption at high temperatures.

The Freundlich coefficient k_F and n are empirical constants, representing the extent and the degree of non-linearity of sorption, respectively. If the constant n has a value of 1, Freundlich isotherm is identical to the linear isotherm. If n is less than 1, the adsorption is a chemical process, otherwise, a physical process [36]. All of the values of n are larger than 1 (Table S3), manifesting physical processes. The k_F value, an indicator of adsorption capacity, becomes larger in

Table 2
Kinetic parameters by Weber–Morris kinetic model for MB adsorption on EDNB/MMt

	Initial linear portion			Second linear portion			Third linear portion		
T (K)	K_{d1}	I_1	R_1	K_{d2}	I_2	R_2	K_{d3}	I_3	R_3
298	37.334	162.729	0.988	21.824	235.172	0.963	0.553	392.959	0.788
308	31.101	199.395	0.976	20.140	249.016	0.975	0.518	393.841	0.792
318	29.421	220.881	0.922	15.133	285.663	0.984	0.351	395.932	0.853
328	28.728	230.084	0.942	10.598	321.160	0.974	0.145	398.233	0.870
338	28.759	265.563	0.967	2.072	384.327	0.878	0.111	398.493	0.788

Table 3
Parameters by Langmuir isotherm for MB adsorption on the improved MMt

	EDNB/MMt					Fe/MMt					EDNB/MMt/Fe				
T (K)	b (L/mg)	R_L ($\times 10^5$)	q_m (mg/g)	R^2	$q_{m,exp}$ (mg/g)	b (L/mg)	R_L ($\times 10^5$)	q_m (mg/g)	R^2	$q_{m,exp}$ (mg/g)	b (L/mg)	R_L ($\times 10^5$)	q_m (mg/g)	R^2	$q_{m,exp}$ (mg/g)
298	0.223	13.95	543.4	0.998	549.0	0.036	2.25	531.9	0.983	545.8	0.030	1.88	512.82	0.980	526.3
308	0.380	23.74	574.7	1.000	570.9	0.035	2.20	529.1	0.977	537.1	0.028	1.72	518.13	0.975	521.9
318	0.803	50.15	584.8	1.000	580.8	0.032	2.02	523.6	0.980	533.3	0.026	1.62	507.61	0.976	514.4
328	1.427	89.13	598.8	1.000	594.8	0.032	1.99	518.1	0.978	531.5	0.026	1.61	507.61	0.969	515.8
338	1.762	110.01	609.7	1.000	605.9	0.029	1.81	518.1	0.984	524.0	0.024	1.53	507.61	0.980	503.2

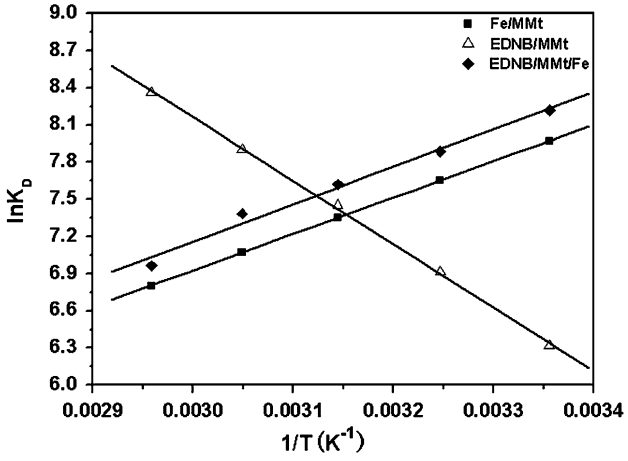

Fig. 10. Plots of Van't Hoff equation for MB adsorption on the improved MMt.

MB-EDNB/MMt system with temperature. The trend is opposite to that in MB-Fe/MMt and in MB-EDNB/MMt/Fe, indicating again that high temperature benefits MB uptake by EDNB/MMt other than by the other two.

Dubinin–Radushkevich isotherm is of temperature independence and more general than the Freundlich and Langmuir models. It predicts the adsorption energy per unit mass of adsorbate and a maximum adsorption capacity. The mean adsorption energy (E) gives information about chemical and physical adsorption. E values (<8 kJ/mol) in Table S4 suggests a physical adsorption process [37]. What is more, for MB on EDNB/MMt, E values increase with raising the temperature, meaning that elevated temperatures may shift the physical process to chemical adsorption. On the contrary, E values decrease with temperature for MB on EDNB/MMt/Fe and on Fe/MMt, which is the feature of physical adsorption.

3.5. Thermodynamics study

The thermodynamic parameters such as standard free energy, ΔG°_{ad}, standard enthalpy, ΔH°_{ad}, and standard entropy, ΔS°_{ad}, are the indicators for practical application of a process and can be acquired by means of the following formulations [38]:

$$K_D = \frac{q_e}{C_e} \tag{12}$$

$$\Delta G^{\circ}_{ad} = -RT \ln K_D \tag{13}$$

$$\ln K_D = -\frac{\Delta H^{\circ}_{ad}}{RT} + \frac{\Delta S^{\circ}_{ad}}{R} \tag{14}$$

$$\Delta G^{\circ}_{ad} = \Delta H^{\circ}_{ad} - T\Delta S^{\circ}_{ad} \tag{15}$$

where K_D is the distribution coefficient of adsorbents, T is the absolute temperature (K) and R is the universal gas constant (8.314 J/mol K). The plot of ln K_D vs. $1/T$ is linear with the slope giving the value of ΔH°_{ad} (Fig. 10).

The thermodynamic parameters are summarized in Table 4. The negative sign of ΔG°_{ad} suggests a spontaneous process with high preference for MB adsorption. In general, ΔG°_{ad} values between 0 and −20 kJ/mol indicate physical adsorption, while those between −80 and −400 kJ/mol correspond to chemiadsorption [39]. For EDNB/MMt, ΔG°_{ad} value shifts more negatively upon incremental temperature. On the contrary, it becomes less negative for EDNB/MMt/Fe and Fe/MMt.

ΔH°_{ad} value is larger than 40 kJ/mol in chemiadsorption while it is less than 40 kJ/mol in physical adsorption [40]. Analyzing the data in Table 4 specifies that MB adsorbing on the EDNB/MMt may belong to chemiadsorption, and it is an endothermic process. However, MB on the EDNB/MMt/Fe and on Fe/MMt follows a physical and exothermic mechanism.

The negative ΔS°_{ad} for MB on EDNB/MMt/Fe and on Fe/MMt demonstrates the decreased randomness of particles at the solid–liquid interface. But the positive ΔS°_{ad} for MB on EDNB/MMt may be due to the hydrophobic interaction between MB and EDNB. This interaction makes more water molecules leaving the surface of EDNB/MMt and leads to a positive enthalpy change during the adsorption [41].

3.6. Regeneration and reuse of the modified MMt

The frequently used reagent for oxidizing organic compounds in the aqueous phase is Fenton H_2O_2–Fe^{2+}/Fe^{3+} [42]. Can MB be easily removed by Fenton reagent on the modified MMt? To test it, we conducted the investigation by UV–vis analysis both in solution and on solid. The result is depicted in Figs. 11 and S16. Fig. S16 specifies that the absorbance of MB diminishes in Fe^{2+}/H_2O_2 solution and almost totally disappears in 2.5 h, confirming thorough decomposition of MB by Fenton reagent. Comparing Fig. 11(a) with Fig. 11(b) suggests a very strong interaction of MB with the adsorbents, especially with EDNB/MMt: enhanced absorbance, broadened and deformed and shifted peaks, and emerged new peaks in the curves. Analyzing the plots in Fig. 11(a) and (c), we can find the almost restored curves (2) and (3), suggesting that

Table 4
Thermodynamic parameters for MB adsorption on the improved MMt

T (K)	EDNB/MMt				Fe/MMt				EDNB/MMt/Fe			
	$\ln K_D$	ΔG°_{ad} (kJ mol^{-1})	ΔS°_{ad} (J mol^{-1})	ΔH°_{ad} (kJ mol^{-1})	$\ln K_D$	ΔG°_{ad} (kJ mol^{-1})	ΔS°_{ad} (J mol^{-1})	ΔH°_{ad} (kJ mol^{-1})	$\ln K_D$	ΔG°_{ad} (kJ mol^{-1})	ΔS°_{ad} (J mol^{-1})	ΔH°_{ad} (kJ mol^{-1})
298	6.317	−15.651	195.46	42.60	7.972	−19.751	−15.819	−24.46	8.217	−20.358	−16.047	−25.14
308	6.914	−17.705	195.78		7.652	−19.594	−15.813		7.888	−20.200	−16.039	
318	7.452	−19.702	195.91		7.354	−19.442	−15.795		7.621	−20.148	−15.697	
328	7.902	−21.548	195.56		7.070	−19.279	−15.809		7.385	−20.140	−15.244	
338	8.363	−23.501	195.56		6.803	−19.117	−15.823		6.964	−19.569	−16.481	

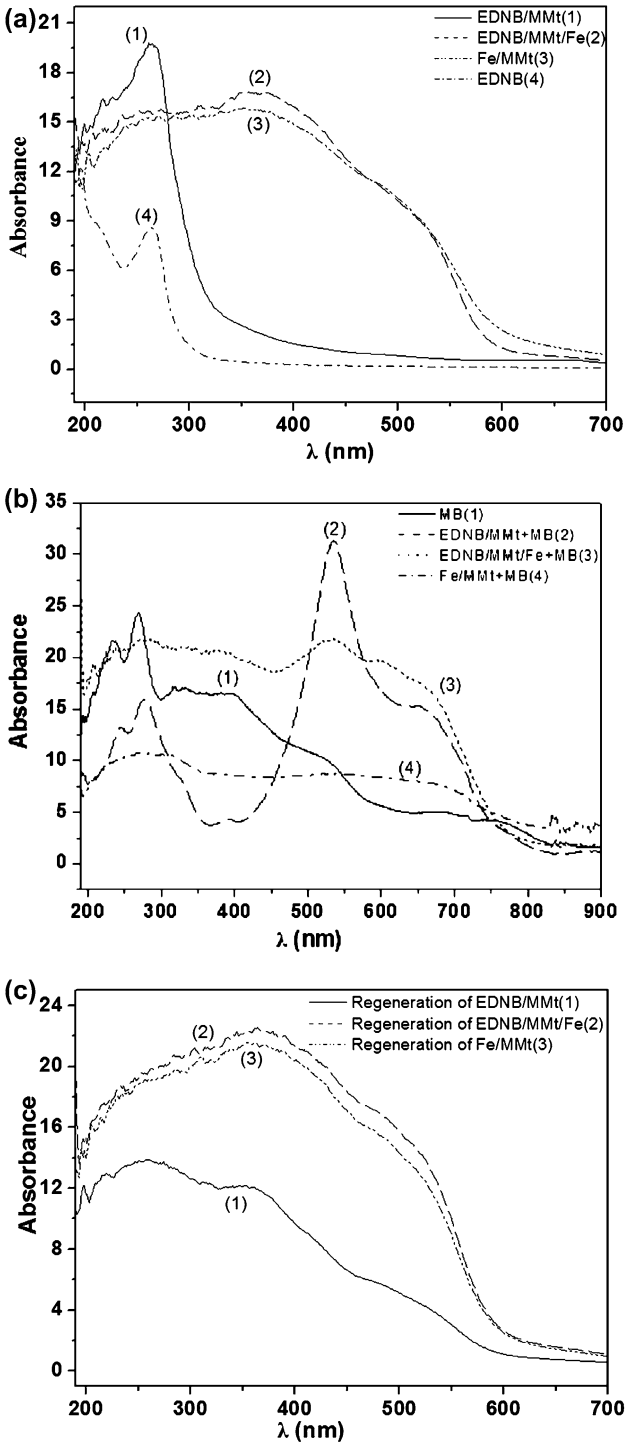

Fig. 11. Solid UV–vis spectra of the improved MMt (a), the improved MMt adsorbed with MB (b), and the regenerated adsorbents after ten cycles (c).

MB has been decomposed on EDNB/MMt/Fe and on Fe/MMt by H_2O_2/Fe^{2+}. The distorted curve (1) is due

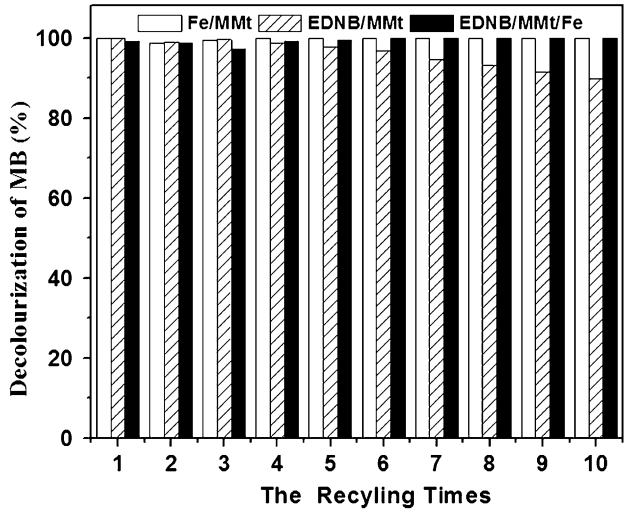

Fig. 12. The recycles of the improved MMt.

to the oxidation and doping of Fe^{3+} or Fe^{2+} because H_2O_2/Fe^{2+} is used as oxidant.

Fig. 12 exhibits that no significant decrease in adsorption capacity of EDNB/MMt/Fe and Fe/MMt is evidenced in ten adsorption/decomposition cycles. MB uptake by EDNB/MMt/Fe (or Fe/MMt) is from 97.1% (or 98.2%) in the first run to 99.9% in the tenth run. However MB uptake by EDNB/MMt lowers gradually in the recycling, from 99.8 to 89.9%, which may be resulted by the surfactant leaking from EDNB/MMt. The result also suggests that MB adsorbed by the three adsorbents has been easily degraded in H_2O_2/Fe^{2+} solution. The regeneration is simple and easy to operate. And MB uptake is almost maintained in multiple adsorptions/regeneration cycles.

It is reported that, despite being highly efficient, the homogeneous iron–peroxide systems have a number of disadvantages restricting their industrial use (for instance, necessary neutralization and separation of iron ions, formation of hydroxide slurries) [43]. However, H_2O_2 and small portion of Fe^{2+} are added in MB/modified MMt suspension in the present work, the disadvantage is addressed because various iron ions produced in the oxidation will intercalate into the clay, together with those already existed in the modified MMt. Therefore, the EDNB/MMt, EDNB/MMt/Fe, and Fe/MMt will be competent for MB removal from the contaminated environment efficiently and cost-effectively.

4. Conclusion

Montmorillonite is modified by EDNB, or by polymeric Fe, or by both the surfactant and polymeric Fe.

The MB uptake capacity and the recycling use of the improved MMt are compared. Following conclusions can be drawn from above discussion.

(1) The three adsorbents removing MB obeys well the pseudo-second-order kinetics model. EDNB/MMt/Fe and Fe/MMt adsorb MB faster than EDNB/MMt does, however, the latter can accommodate more MB at the same dosage, suggesting that the hydrophobic interaction and π–π stacking play roles in the adsorption besides electrostatic attraction. The intraparticle diffusion is not the only rate-limiting step, and the external mass transfer is also important in controlling the adsorption rate. Generally, MB adsorbing on EDNB/MMt follows well Weber−Morris intraparticle diffusion model due to the slower adsorption.
(2) The three adsorbents removing MB fits well Langmuir isotherm with good agreement of $q_{m,cal}$ with $q_{m,exp}$. ΔG°_{ad} value becomes more negative with elevated temperature for MB on EDNB/MMt, but it exhibits the contrary on EDNB/MMt/Fe and on Fe/MMt, manifesting that elevated temperature benefits the adsorption of MB on the surfactant-modified MMt. The values of both ΔH°_{ad} and ΔS°_{ad} are positive for MB/EDNB/MMt, but negative for MB/EDNB/MMt/Fe and MB/Fe/MMt, indicating that EDNB/MMt removes MB through enthalpy driving and chemical adsorption, and that EDNB/MMt/Fe and Fe/MMt gets rid of MB by physical adsorption.
(3) MB can be easily *in situ* decomposed by Fenton reagent, and the adsorbents can be reused at least ten times without obvious decrease in MB uptake. And, EDNB/MMt/Fe and Fe/MMt are more ready to be regenerated and recycled than EDNB/MMt. Due to the existence of the adsorbents, the drawback of Fenton reagent is addressed. So, adsorption coupled with *in situ* Fenton oxidation leads to MB being easily removed from the contaminated circumstance, and this study offers new idea in dye wastewater treatment.

Supplementary material

The supplementary material for this paper is available online at http://dx.doi.10.1080/19443994.2015.1088896.

Acknowledgments

The authors are very grateful for financial supports from the National Natural Science Foundation of China (21176201).

References

[1] D. Sannino, V. Vaiano, O. Sacco, P. Ciambelli, Mathematical modelling of photocatalytic degradation of methylene blue under visible light irradiation, J. Environ. Chem. Eng. 1 (2013) 56–60.
[2] J. Sheng, Y. Xie, Y. Zhou, Adsorption of methylene blue from aqueous solution on pyrophyllite, Appl. Clay Sci. 46 (2009) 422–424.
[3] E. Haque, J.W. Jun, S.H. Jhung, Adsorptive removal of methyl orange and methylene blue from aqueous solution with a metal-organic framework material, iron terephthalate (MOF-235), J. Hazard. Mater. 185 (2011) 507–511.
[4] E. Rossetto, D.I. Petkowicz, J.H.Z. dos Santos, S.B.C. Pergher, F.G. Penha, Bentonites impregnated with TiO_2 for photodegradation of methylene blue, Appl. Clay Sci. 48 (2010) 602–606.
[5] B. Yuan, J. Xu, X. Li, M. Fu, Preparation of Si–Al/α-FeOOH catalyst from an iron-containing waste and surface-catalytic oxidation of methylene blue at neutral pH value in the presence of H_2O_2, Chem. Eng. J. 226 (2013) 181–188.
[6] F. Nerud, P. Baldrian, I. Eichlerová, V. Merhautová, J. Gabriel, L. Homolka, Decolorization of dyes using white-rot fungi and radical-generating reactions, Biocatal. Biotransform. 22 (2004) 325–330.
[7] Y. Li, Q. Du, T. Liu, X. Peng, J. Wang, J. Sun, Y. Wang, S. Wu, Z. Wang, Y. Xia, L. Xia, Comparative study of methylene blue dye adsorption onto activated carbon, graphene oxide, and carbon nanotubes, Chem. Eng. Res. Des. 91 (2013) 361–368.
[8] M. Hajjaji, H. El Arfaoui, Adsorption of methylene blue and zinc ions on raw and acid-activated bentonite from Morocco, Appl. Clay Sci. 46 (2009) 418–421.
[9] Y. El Mouzdahir, A. Elmchaouri, R. Mahboub, A. Gil, S.A. Korili, Equilibrium modeling for the adsorption of methylene blue from aqueous solutions on activated clay minerals, Desalination 250 (2010) 335–338.
[10] C. Cheng, J. Deng, B. Lei, A. He, X. Zhang, L. Ma, S. Li, C. Zhao, Toward 3D graphene oxide gels based adsorbents for high-efficient water treatment via the promotion of biopolymers, J. Hazard. Mater. 263 (2013) 467–478.
[11] G.K. Sarma, S.S. Gupta, K.G. Bhattacharyya, Methylene blue adsorption on natural and modified clays, Sep. Sci. Technol. 46 (2011) 1602–1614.
[12] C.A.P. Almeida, N.A. Debacher, A.J. Downs, L. Cottet, C.A.D. Mello, Removal of methylene blue from colored effluents by adsorption on montmorillonite clay, J. Colloid Interface Sci. 332 (2009) 46–53.
[13] W.S. Shin, Competitive sorption of anionic and cationic dyes onto cetylpyridinium-modified montmorillonite, J. Environ. Sci. Health 43 (2008) 1459–1470.

[14] A.A. Tireli, F.C.F. Marcos, L.F. Oliveira, I. do R. Guimarãesa, M.C. Guerreiroa, J.P. Silva, Influence of magnetic field on the adsorption of organic compound by clays modified with iron, Appl. Clay Sci. 97–98 (2014) 1–7.
[15] A. Gil, F.C.C. Assis, S. Albeniz, S.A. Korili, Removal of dyes from wastewaters by adsorption on pillared clays, Chem. Eng. J. 168 (2011) 1032–1040.
[16] S. Li, P. Wu, Characterization of sodium dodecyl sulfate modified iron pillared montmorillonite and its application for the removal of aqueous Cu(II) and Co (II), J. Hazard. Mater. 173 (2010) 62–70.
[17] J. Jiang, C. Cooper, S. Ouki, Comparison of modified montmorillonite adsorbents. Part I: Preparation, characterization and phenol adsorption, Chemosphere 47 (2002) 711–716.
[18] J.L. Marco-Brown, C.M. Barbosa-Lema, R.M.T. Sánchez, R.C. Mercader, M. dos S. Afonso, Adsorption of picloram herbicide on iron oxide pillared montmorillonite, Appl. Clay Sci. 58 (2012) 25–33.
[19] A. Gürses, C. Doğar, M. Yalçin, M. Açikyildiz, R. Bayrak, S. Karaca, The adsorption kinetics of the cationic dye, methylene blue, onto clay, J. Hazard. Mater. B 131 (2006) 217–228.
[20] J. Zhang, D. Cai, G. Zhang, C. Cai, C. Zhang, G. Qiu, K. Zheng, Z. Wu, Adsorption of methylene blue from aqueous solution onto multiporous palygorskite modified by ion beam bombardment: Effect of contact time, temperature, pH and ionic strength, Appl. Clay Sci. 83–84 (2013) 137–143.
[21] O. Bouras, J. Bollinger, M. Baudu, H. Khalaf, Adsorption of diuron and its degradation products from aqueous solution by surfactant-modified pillared clays, Appl. Clay Sci. 37 (2007) 240–250.
[22] R. Zhang, W. Yan, C. Jing, Mechanistic study of PFOS adsorption on kaolinite and montmorillonite, Colloids Surf., A 462 (2014) 252–258.
[23] M.L. Lay, H.M. Wu, Study of the zeta potential of Fe (O)OH colloids, J. Mater. Sci. 30 (1995) 5473–5478.
[24] Y. Wang, J. Duan, S. Liu, W. Li, J. van Leeuwen, D. Mulcahy, Removal of As(III) and As(V) by ferric salts coagulation—Implications of particle size and zeta potential of precipitates, Sep. Purif. Technol. 135 (2014) 64–71.
[25] Y. Ho, Review of second-order models for adsorption systems, J. Hazard. Mater. B 136 (2006) 681–689.
[26] L. Zhang, P. Fang, L. Yang, J. Zhang, X. Wang, Rapid method for the separation and recovery of endocrine-disrupting compound bisphenol AP from wastewater, Langmuir 29 (2013) 3968–3975.
[27] K. Rida, S. Bouraoui, S. Hadnine, Adsorption of methylene blue from aqueous solution by kaolin and zeolite, Appl. Clay Sci. 83–84 (2013) 99–105.
[28] A. Roy, B. Adhikari, S.B. Majumder, Equilibrium, kinetic, and thermodynamic studies of azo dye adsorption from aqueous solution by chemically modified lignocellulosic jute fiber, Ind. Eng. Chem. Res. 52 (2013) 6502–6512.
[29] Y.H. Shu, L.S. Li, Q.Y. Zhang, H.H. Wu, Equilibrium, kinetics and thermodynamic studies for sorption of chlorobenzenes on CTMAB modified bentonite and kaolinite, J. Hazard. Mater. 173 (2010) 47–53.
[30] G. Xue, M. Gao, Z. Gu, Z. Luo, Z. Hu, The removal of p-nitrophenol from aqueous solutions by adsorption using gemini surfactants modified montmorillonites, Chem. Eng. J. 218 (2013) 223–231.
[31] J.C.P. Vaghetti, E.C. Lima, B. Royer, B.M. da Cunha, N.F. Cardoso, J.L. Brasil, S.L.P. Dias, Pecan nutshell as biosorbent to remove Cu(II), Mn(II) and Pb(II) from aqueous solutions, J. Hazard. Mater. 162 (2009) 270–280.
[32] F. Yu, Y. Wu, X. Li, J. Ma, Kinetic and thermodynamic studies of toluene, ethylbenzene, and m-xylene adsorption from aqueous solutions onto KOH-activated multiwalled carbon nanotubes, J. Agric. Food Chem. 60 (2012) 12245–12253.
[33] N.A. Travlou, G.Z. Kyzas, N.K. Lazaridis, E.A. Deliyanni, Functionalization of graphite oxide with magnetic chitosan for the preparation of a nanocomposite dye adsorbent, Langmuir 29 (2013) 1657–1668.
[34] H. Yan, H. Li, H. Yang, A. Li, R. Cheng, Removal of various cationic dyes from aqueous solutions using a kind of fully biodegradable magnetic composite microsphere, Chem. Eng. J. 223 (2013) 402–411.
[35] Y. Liu, Y. Kang, B. Mu, A. Wang, Attapulgite/bentonite interactions for methylene blue adsorption characteristics from aqueous solution, Chem. Eng. J. 237 (2014) 403–410.
[36] Q. Wen, Z. Chen, J. Lian, Y. Feng, N. Ren, Removal of nitrobenzene from aqueous solution by a novel lipoid adsorption material (LAM), J. Hazard. Mater. 209–210 (2012) 226–232.
[37] A. Olgun, N. Atar, Equilibrium and kinetic adsorption study of Basic Yellow 28 and Basic Red 46 by a boron industry waste, J. Hazard. Mater. 161 (2009) 148–156.
[38] T. Liu, Y. Li, Q. Du, J. Sun, Y. Jiao, G. Yang, Z. Wang, Y. Xia, W. Zhang, K. Wang, H. Zhu, D. Wu, Adsorption of methylene blue from aqueous solution by grapheme, Colloids Surf., B 90 (2012) 197–203.
[39] M. Auta, B.H. Hameed, Modified mesoporous clay adsorbent for adsorption isotherm and kinetics of methylene blue, Chem. Eng. J. 198–199 (2012) 219–227.
[40] C. Kannan, K. Muthuraja, M.R. Devi, Hazardous dyes removal from aqueous solution over mesoporous aluminophosphate with textural porosity by adsorption, J. Hazard. Mater. 244–245 (2013) 10–20.
[41] Y. Wang, X. Jiang, L. Zhou, C. Wang, Y. Liao, M. Duan, X. Jiang, A comparison of new gemini surfactant modified clay with its monomer modified one: Characterization and application in methyl orange removal, J. Chem. Eng. Data 58 (2013) 1760–1771.
[42] E.T. Dashinamzhilova, S.T. Khankhasaeva, Use of intercalated clays in oxidation of organic dyes, Russ. J. Appl. Chem. 84 (2011) 1207–1212.
[43] P. Yuan, F. Annabi-Bergaya, Q. Tao, M. Fan, Z. Liu, J. Zhu, H. He, T.A. Chen, A combined study by XRD, FTIR, TG and HRTEM on the structure of delaminated Fe-intercalated/pillared clay, J. Colloid Interface Sci. 324 (2008) 142–149.